Mathematical Biology

CrossMark

Mathematical modeling and simulation of the evolution of plaques in blood vessels

Yifan Yang[1] · **Willi Jäger**[1] · **Maria Neuss-Radu**[2] · **Thomas Richter**[3]

Abstract In this paper, a model is developed for the evolution of plaques in arteries, which is one of the main causes for the blockage of blood flow. Plaque rupture and spread of torn-off material may cause closures in the down-stream vessel system and lead to ischemic brain or myocardial infarctions. The model covers the flow of blood and its interaction with the vessel wall. It is based on the assumption that the penetration of monocytes from the blood flow into the vessel wall, and the accumulation of foam cells increasing the volume, are main factors for the growth of plaques. The dynamics of the vessel wall is governed by a deformation gradient, which is given as composition of a purely elastic tensor, and a tensor modeling the biologically caused volume growth. An equation for the evolution of the metric is derived quantifying the changing geometry of the vessel wall. To calculate numerically the solutions of the arising free

Dedicated to Mats Gyllenberg on the occasion of his 60th birthday.

✉ Maria Neuss-Radu
  maria.neuss-radu@math.fau.de

  Yifan Yang
  yifan.yang@iwr.uni-heidelberg.de

  Willi Jäger
  wjaeger@iwr.uni-heidelberg.de

  Thomas Richter
  thomas.richter@iwr.uni-heidelberg.de

[1] Interdisciplinary Center for Scientific Computing, Heidelberg University, Im Neuenheimer Feld 368, 69120 Heidelberg, Germany

[2] Mathematics Department, University of Erlangen-Nuremberg, Cauerstr. 11, 91058 Erlangen, Germany

[3] Institute for Applied Mathematics, Heidelberg University, Im Neuenheimer Feld 294, 69120 Heidelberg, Germany

boundary problem, the model system of partial differential equations is transformed to an ALE (Arbitrary Lagrangian-Eulerian) formulation, where all equations are given in fixed domains. The numerical calculations are using newly developed algorithms for ALE systems. The results of the simulations, obtained for realistic system parameters, are in good qualitative agreement with observations. They demonstrate that the basic modeling assumption can be justified. The increase of stresses in the vessel wall can be computed. Medical treatment tries to prevent critical stress values, which may cause plaque rupture and its consequences.

Keywords Atherosclerotic plaque formation · Fluid-structure interaction · Coupling biochemical reactions and biomechanics · Modeling tissue growth · Computing wall stresses

Mathematics Subject Classification 35Q30 · 74L15 · 92C10 · 92C50

1 Introduction

Atherosclerosis is a far spread disease of arteries and is related to coronary artery disease, stroke and other conditions. It is linked to build up of cholesterol in the vessel walls and the formation of plaques, which are in general slow processes, however in their consequences may be dangerous. Plaques are formed primarily in the inner-most layer of the vessel the wall, the intima. They might rupture and become partially detached. Their formation is initiated by endothelial dysfunction, and involves several biochemical processes. This investigation is concentrating on the most important subprocesses, described in the following. Leucocytes, in particular monocytes, from the blood flow are attracted to the vessel wall. They migrate into the inflamed intima. Here, a cytokine, known as macrophage colony-stimulating factor, induces the differentiation of monocytes to macrophages. These immune cells take up low-density lipoproteins, which carry cholesterol and triglycerides to the tissues, and are finally transformed into foam cells, which are engorged with lipids Hahn and Schwartz (2009).

The accumulation of foam cells in the vessel causes a swelling of the vessel walls. The subsequent evolution of the plaques consists of formation of structures and components typical for a mature plaque: a soft, lipid-rich atheromatous core and a hard, collagen-rich sclerotic tissue, called fibrous cap Pasterkamp and Falk (2000). It is generally believed that the death of foam cells plays an important role in lipid accumulation and core formation, making the plaque vulnerable to rupture. The fibrous cap is produced mainly by smooth muscle cells. It stabilizes the plaque by separating the lipid core from the vessel lumen.

A plaque with a large core and a thin cap becomes vulnerable and may rupture, if the biomechanical forces reach a critical value. After plaque rupture, platelets in the blood to the flow adhere to the ruptured region and lead to thrombus formation Fasano et al. (2011), Weller (2008), Weller et al. (2013). Plaques and thrombi reduce blood flow, and may lead to blood clots and to partial or complete occlusions of vessels firstly locally. However torn-off material of ruptured plaques may cause closures in the down-stream vessel system and lead to ischemic brain or myocardial infarctions. Blocking blood

supply is blocking oxygen supply. Hypoxia is causing a chain of processes, leading to damages of the tissue and vessel system, which might become irreparable. In fact, the following question, posed by neurologists involved with prevention and treatment of brain infarctions, inspired the investigation presented in this paper: *Is it possible to develop and simulate a mathematical model for plaque formation and to compute the stresses in the plaque region, providing information on an impending rupture?*

The network of biochemical, biophysical and biomechanical processes taking place is huge and complex. Depending on the questions to be answered, reduced mathematical models have to be developed VanEpps and Vorp (2007). Whereas there has been substantial progress in modelling and simulation of pure fluid-structure interaction for blood flow in vessels with prescribed mechanics of deformable vessel walls, research including process dependent changes of the shape and the properties of the vessel wall is only at its initial stages. Models based on the fluid-structure interaction between blood flow and vessel wall without plaques are given e.g. in Formaggia et al. (2007), Janela et al. (2010), Wick (2011), Hron and Madlik (2007), Turek et al. (2010). In Tang et al. (2004, 2009) fluid-structure interaction models are considered, where the constitutive equations describing material properties of the vessel wall include information on plaque components. The stress distributions obtained by the simulation of these models are used for possible plaque rupture predictions. On the other hand, mathematical models have been devised to study the role of the biochemical processes in the formation of plaques. They are based on partial or ordinary differential equations, describing the reactions between immune cells (primarily macrophages), smooth muscle cells, chemo-attractant and low-density lipoproteins, see e.g. Khatib et al. (2007), Ibragimov et al. (2005), Ougrinovskaia et al. (2010). In Zohdi et al. (2004), a phenomenological model, which accounts for the intimal thickening due to adhesion of monocytes to the intima surface is developed.

The main purpose of this paper is to derive a reduced model describing the evolution from healthy tissue to a mature plaque, which may rupture. The crucial contribution of this investigation is modeling the growth of the vessel wall due to accumulation of foam cells. It has to be considered as a first step, leading to the features of plaque formation as observed in reality. The model integrates the fluid dynamical, mechanical and chemical interactions of blood, cells, tissues and chemical substances important for signaling. The formation of a liquid core and fibrous cap is not explicitly modelled. The activities of monocytes, macrophages and foam cells are in the focus of this investigation.

The mathematical model consists of two main parts. For the description of the biomechanical interaction between the blood flow and the vessel wall, we use the fluid-structure interaction problem with the Navier-Stokes equations for fluids and the elastic structure equations for solids. To describe the dynamics and biochemical reactions of monocytes, macrophages and foam cells we use the transport equations. These two problems are coupled with growth modelling. The equation for the metric of growth is related to the growth and reaction functions in solids, and the stress tensor in the elastic structure equations is obtained by this metric and the constitutive equations. Moreover, the model assumes that the increase of the concentration of foam cells not only lets the volume of solid phase grow, but also changes its mechanical properties. The main results of the paper can be summarized as follows:

- The simulation of the model equations demonstrate numerically that under realistic assumptions on the system parameters, the resulting formation of plaques is in good agreement with the observations, as far as the dynamics and the shape of the plaques are concerned.
- Numerical methods were developed to compute relevant information, in particular the dynamics of monocytes, foam cells and stresses in the deforming vessel walls.

Our investigation has shown that the reduced model is able to capture main features of the plaque formation. However, they also suggest to refine the model in several directions, integrating the continually increasing information on the underlying processes. So far simulations were performed only in 2 dimensions. The step into 3d is just in preparation. The developed numerical methods will be published in an independent paper, see [41]. They are based on an ALE reformulation, reducing a free boundary problem for a system of nonlinear partial differential equations to a system in fixed domains. The full mathematical analysis of the resulting system remains to be done in future research. The paper is structured as follows. Section 2 explains step by step the detailed modeling procedure and provides the final model. Section 3 introduces the Arbitrary Lagrangian-Eulerian (ALE) framework, lists the numerical methods to simulate the model and presents the numerical results. Section 4 concludes the paper and provides an outlook for future development.

2 Mathematical model

In this section, we formulate a mathematical model which describes the biochemical and biomechanical processes leading to formation and growth of plaques in blood vessels. We consider a domain $\Omega \subset \mathbb{R}^2$ which at every time t consists of two subdomains Ω_f^t and Ω_s^t, separated by an interface Γ^t, see also Fig. 1. The fluid domain Ω_f^t represents the part occupied by the blood, and the solid domain Ω_s^t represents the part occupied by the vessel wall. The interface Γ^t is given as $\Gamma^t = \Gamma_1^t \cup \Gamma_2^t$. Here Γ_1^t represents the diseased part of the interface, and it is permeable for the monocytes. The interface Γ_2^t represents the healthy part of the interface Γ^t. There is another interface between blood and vessel wall, denoted by $\Gamma_{f,wall}$ which is a subset of the boundary $\partial\Omega$, see again Fig. 1. However, since this part is not diseased, we suppose that its displacement is small compared to the displacement of $\Gamma_1^t \cup \Gamma_2^t$ (which is supposed

Fig. 1 Computational domain
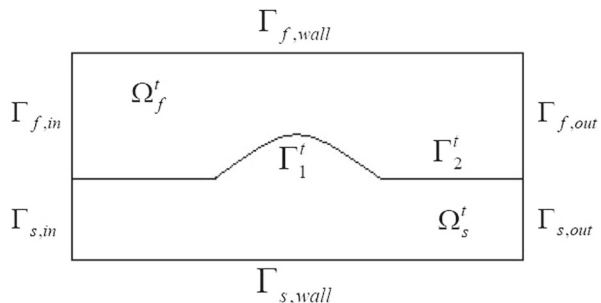
to move due to penetration of monocytes and accumulation of foam cells). Therefore the boundary $\Gamma_{f,wall}$ is supposed to be fixed. The remaining parts of $\partial\Omega$, namely $\Gamma_{s,wall} \cup \Gamma_{s,in} \cup \Gamma_{s,out}$, $\Gamma_{f,in}$, and $\Gamma_{f,out}$ denote the interface between the vessel wall and the tissue surrounding the blood vessel, the inflow and the outflow boundary, respectively. They are all assumed to be fixed.

2.1 Fluid-structure interaction

Let us start by formulating the balance equations of mass and momentum for fluid dynamics as well as for structural mechanics. Hereby, the quantities defined on the fluid domain are marked by a lower index f, whereas those defined on the solid domain are distinguished by a lower index s. Let the deformation x be a smooth, orientation preserving and one-to-one mapping

$$x(\cdot, t) : \Omega^0 \to \Omega^t, \quad X \mapsto x = x(X, t), \quad t \in I = [0, T],$$

and let its inverse be denoted by $X(\cdot, t)$. The couple (x, t) is called Eulerian variables, and the couple (X, t) is called Lagrangian variables. A physical or chemical quantity can be described either as a function $\phi(x, t)$ or $\hat{\phi}(X, t)$. Quantities associated to fluids are usually described with respect to Eulerian framework whereas quantities occurring in solids are usually described with respect to Lagrangian framework.

We assume that the blood flow is an incompressible Newtonian fluid, assumption which is generally valid in large vessels Quarteroni and Formaggia (2004). Thus, the pressure p_f and the velocity $\mathbf{v}_f$ of the blood flow are described by the Navier-Stokes equations

$$\operatorname{div}\mathbf{v}_f = 0 \quad \text{in} \quad \Omega^t_f$$
$$\rho_f \frac{\partial \mathbf{v}_f}{\partial t} + \rho_f \mathbf{v}_f \cdot \nabla \mathbf{v}_f = \operatorname{div}\boldsymbol{\sigma}_f \quad \text{in} \quad \Omega^t_f. \tag{1}$$

Since the blood flow is assumed to be homogeneous, the density ρ_f is constant. The stress tensor $\boldsymbol{\sigma}_f$ is defined as

$$\boldsymbol{\sigma}_f = -p_f I + \rho_f \nu (\nabla \mathbf{v}_f + \nabla \mathbf{v}_f^T) \quad \text{in} \quad \Omega^t_f, \tag{2}$$

where ν is the kinematic viscosity. The fluid problem is written with respect to Eulerian variables in the current configuration on the moving domain Ω^t_f.

In contrast, elastic solids are usually described in the fixed reference system Ω^0_s, in the Lagrangian reference frame. We denote the displacement by

$$\hat{\mathbf{u}}(\cdot, t) : \Omega^0 \to \Omega^t, \quad X \mapsto \hat{\mathbf{u}}(X, t) = x(X, t) - X, \quad t \in I = [0, T],$$

and the velocity by

$$\hat{\mathbf{v}}(X, t) = \frac{\partial}{\partial t} x(X, t) = \frac{\partial}{\partial t} \hat{\mathbf{u}}(X, t), \quad X \in \Omega^0, t \in I.$$

Finally, we denote by $\hat{\mathbf{F}}$ the deformation gradient

$$\hat{\mathbf{F}} = \frac{\partial}{\partial X} x(X, t) = \hat{\nabla} x(X, t) = I + \hat{\nabla}\hat{\mathbf{u}}(X, t), \quad X \in \Omega^0, t \in I,$$

where the symbol $\hat{\nabla}$ indicates the gradient with respect to the Lagrangian variable X. Since the deformation is supposed to be smooth, injective and orientation preserving, the deformation gradient $\hat{\mathbf{F}}$ is invertible and its determinant

$$\hat{J} = \det\hat{\mathbf{F}} \tag{3}$$

is everywhere strictly positive, see e.g. Ciarlet (1988).

The equations for structural mechanics, describing the displacement $\hat{\mathbf{u}}_s$ and the velocity $\hat{\mathbf{v}}_s$ of the vessel wall, are written with respect to Lagrangian variables as follows

$$\begin{aligned}
\frac{\partial}{\partial t}(\hat{J}_s \hat{\rho}_s) &= \hat{J}_s \hat{f}_s^g \quad \text{in} \quad \Omega_s^0 \\
\hat{J}_s \hat{\rho}_s \frac{\partial \hat{\mathbf{v}}_s}{\partial t} &= \widehat{\text{div}}(\hat{J}_s \hat{\boldsymbol{\sigma}}_s \hat{\mathbf{F}}_s^{-T}) \quad \text{in} \quad \Omega_s^0 \\
\frac{\partial \hat{\mathbf{u}}_s}{\partial t} &= \hat{\mathbf{v}}_s \quad \text{in} \quad \Omega_s^0.
\end{aligned} \tag{4}$$

The first equation is the mass balance equation. The function $\hat{f}_s^g$ is called growth function, and represents the rate of mass growth per unit reference volume due to the formation of the plaque. We will describe this function in more details in the next section dedicated to the biochemical processes, see (12). The second equation is the balance equation of momentum. The Cauchy stress tensor $\hat{\boldsymbol{\sigma}}_s$ depends on the displacement $\hat{\mathbf{u}}_s$, and will be derived in Sect. 2.3. The conservation equation of energy and the entropy inequality are neglected because both the blood flow and the vessel wall are assumed to be isothermal.

The interaction between the blood flow and the vessel wall is modeled by transmission conditions on the interface $\Gamma^t = \Gamma_1^t \cup \Gamma_2^t$. We impose the natural conditions, namely the continuity of velocity and the balance of forces:

$$\mathbf{v}_f = \mathbf{v}_s, \quad \boldsymbol{\sigma}_f \cdot \mathbf{n}_f + \boldsymbol{\sigma}_s \cdot \mathbf{n}_s = 0, \quad \text{on} \quad \Gamma^t. \tag{5}$$

Here $\mathbf{n}_f$ and $\mathbf{n}_s$ are the unit outer normal vectors of the interface Γ^t with respect to Ω_f^t and Ω_s^t.

2.2 Biochemical processes

For the biochemical processes, in our model, we describe the dynamics of monocytes (with concentration c_f) in the blood flow, and the dynamics of macrophages and foam cells in the vessel wall. The concentrations of the latter are denoted by c_s respectively

c_s^*. The motion of monocytes in the blood is due to convection with the velocity $\mathbf{v}_f$, and diffusion with the diffusion coefficient D_f. It is described by the following transport equation:

$$\frac{\partial c_f}{\partial t} + \operatorname{div}(c_f \mathbf{v}_f) - D_f \triangle c_f = 0 \quad \text{in} \quad \Omega_f^t. \tag{6}$$

The equation for the motion of macrophages in the vessel wall is given by a similar transport equation. However, on the right hand side, we have a reaction term, denoted by $-f_s^r$, describing the rate of transformation of macrophages into foam cells. Concerning the foam cells, since they don't diffuse inside the wall, their accumulation is described by a balance equation involving a production rate equal to f_s^r.

$$\frac{\partial c_s}{\partial t} + \operatorname{div}(c_s \mathbf{v}_s) - \operatorname{div}(D_s \nabla c_s) = -f_s^r \quad \text{in} \quad \Omega_s^t \tag{7}$$

$$\frac{\partial c_s^*}{\partial t} + \operatorname{div}(c_s^* \mathbf{v}_s) = f_s^r \quad \text{in} \quad \Omega_s^t. \tag{8}$$

Since the material properties of the plaque are different from those of the healthy vessel wall, Ω_s^t is not considered a homogeneous material, and thus D_s is not constant. In particular, it depends on the concentration of foam cells c_s^*, and we assume

$$D_s = D_{s,d} + (D_{s,h} - D_{s,d}) f(c_s^*) \quad \text{in} \quad \Omega_s^t. \tag{9}$$

Here, $D_{s,d}$ denotes the diffusion coefficient in the diseased vessel wall occupied by the plaque, and containing a high concentration of foam cells, and $D_{s,h}$ denotes the diffusion coefficient in the healthy vessel wall, where there are no foam cells. The function f in (9) is a continuous monotonic function dependent on the concentration of foam cells c_s^*. When $c_s^* = 0$, f should be equal to 1, and $D_s = D_{s,h}$. As c_s^* is increasing, f should rapidly decrease to zero limit and D_s is getting very close to $D_{s,d}$. For this purpose we define f as an exponential function and (9) can be written as

$$D_s = D_{s,d} + (D_{s,h} - D_{s,d}) e^{-a_1 c_s^*} \quad \text{in} \quad \Omega_s^t. \tag{10}$$

Here $a_1 > 0$ is a constant. We remark that representations similar to (9) are also used for shear-rate dependent viscosity in the modeling of non-Newtonian fluids, see e.g. Boyd et al. (2007), Janela et al. (2010), Robertson et al. (2008).

Concerning the reaction function f_s^r, we assume a linear dependence on the concentration of macrophages c_s:

$$f_s^r = \beta c_s \quad \text{in} \quad \Omega_s^t. \tag{11}$$

Hereby, we consider the coefficient $\beta > 0$ to be a constant. In general, it may depend on the concentration of other chemical species (e.g. low-density lipoproteins), see e.g. Fogelson (1992), Ibragimov et al. (2005). Since the accumulation of foam cells leads

to plaque growth, the growth function f_s^r is also related to f_s^g. We assume a linear relation given by

$$f_s^g = \gamma f_s^r \quad \text{in} \quad \Omega_s^t \tag{12}$$

with a constant coefficient $\gamma > 0$.

Equations (7) and (8) can also be transformed to the Lagrangian framework as (4). Taking into account the transformation formula for the gradients $\nabla \phi = \hat{\mathbf{F}}^{-T} \hat{\nabla} \hat{\phi}$, for a smooth scalar function $\phi = \phi(x, t)$, and using again the Piola transformation, we obtain

$$\frac{\partial}{\partial t} (\hat{J}_s \hat{c}_s) - \widehat{\operatorname{div}} (\hat{J}_s \hat{\mathbf{F}}_s^{-1} \cdot \hat{D}_s \hat{\mathbf{F}}_s^{-T} \hat{\nabla} \hat{c}_s) = -\hat{J}_s \hat{f}_s^r \quad \text{in} \quad \Omega_s^0 \tag{13}$$

$$\frac{\partial}{\partial t} (\hat{J}_s \hat{c}_s^*) = \hat{J}_s \hat{f}_s^r \quad \text{in} \quad \Omega_s^0. \tag{14}$$

The penetration of monocytes from the blood flow into the vessel wall is modeled by transmission conditions for the concentration of monocytes c_f and of macrophages c_s on the interface Γ^t

$$\begin{aligned} D_f \nabla c_f \cdot \mathbf{n}_f + D_s \nabla c_s \cdot \mathbf{n}_s &= 0, \quad \text{on} \quad \Gamma^t \\ D_f \nabla c_f \cdot \mathbf{n}_f + \zeta (c_f - c_s) &= 0, \quad \text{on} \quad \Gamma^t. \end{aligned} \tag{15}$$

These conditions describe the continuity of the normal fluxes across Γ^t. Moreover, the flux is related to the difference of concentrations across the interface. Similar transmission conditions can be found e.g. in Quarteroni et al. (2001). The coefficient ζ describes the permeability of the interface Γ^t with respect to the monocytes. Therefore $\zeta = 0$ on the healthy part Γ_2^t.

2.3 Stress tensor modeling

In this section, we derive the constitutive equations, which relate the stress tensor $\boldsymbol{\sigma}_s$ to the deformation gradient $\mathbf{F}_s$. We consider the vessel wall to be modeled as an elastic and homogeneous material, thus the Cauchy stress tensor $\boldsymbol{\sigma}_s$ depends only on the deformation gradient. However, since in our application the deformation is induced both by growth and mechanics, only the deformation induced by elastic response contributes to the stress loading of the material. Figure 2 is a simple thought experiment to clarify this aspect. Let a force N be applied on the elastic rod. In mechanical equilibrium N is proportional to the observed displacement of the rod $\triangle L$ and can be calculated by measuring $\triangle L$. However, if for some reason the same rod is able to grow, there will be some new elements formed inside the rod when it is deformed by a force N. Then the observed displacement $\triangle L$ is not proportional to N anymore and it is not appropriate for calculating N.

To overcome this problem, we decompose the deformation gradient $\hat{\mathbf{F}}_s$ into two parts: the first one takes care of purely elastic response $\hat{\mathbf{F}}_s^e$ and the second one is
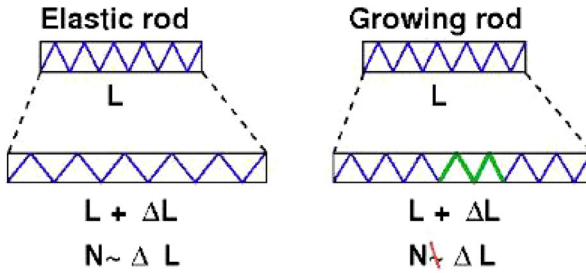
Fig. 2 A thought experiment to show how growth may falsify the usual way of quantifying the deformation. From Doktorski (2007)
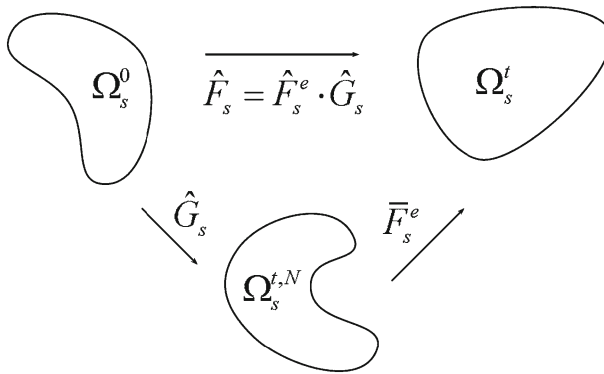

Fig. 3 Decomposition of deformation gradient

connected to the deformation due to growth $\hat{\mathbf{G}}_s$. In doing so, we follow the approach of multiple natural configurations, see e.g. Ambrosi and Mollica (2002), Jones and Chapman (2012), Rajagopal and Srinivasa (2004). Hereby a new configuration, called natural configuration $\Omega_s^{t,N}$, is introduced, see Fig. 3, such that Ω_s^0 is deformed to $\Omega_s^{t,N}$ at first with deformation gradient $\hat{\mathbf{G}}_s$, and then to Ω_s^t with deformation gradient $\hat{\mathbf{F}}_s^e$. We suppose that $\hat{\mathbf{G}}_s$ and $\hat{\mathbf{F}}_s^e$ are invertible and thus the whole deformation gradient $\hat{\mathbf{F}}_s$ is decomposed as

$$\hat{\mathbf{F}}_s = \hat{\mathbf{F}}_s^e \hat{\mathbf{G}}_s \quad \text{in} \quad \Omega_s^0. \tag{16}$$

Here

$$\hat{\mathbf{F}}_s^e = \hat{\mathbf{F}}_s^e(X, t) = \bar{\mathbf{F}}_s^e(X_N(X, t), t), \quad X \in \Omega_s^0, t \in I,$$

and

$$\bar{\mathbf{F}}_s^e = \frac{\partial}{\partial X_N} \tilde{x}(X_N, t), \quad X_N \in \Omega_s^{t,N}, t \in I,$$

where the mapping $\tilde{x}(\cdot, t)$ is defined as

$$\tilde{x}(\cdot, t) : \Omega_s^{t,N} \rightarrow \Omega_s^t,$$
$$X_N = X_N(X, t) \mapsto \tilde{x}(X_N, t) = x(X, t), \quad t \in I = [0, T].$$

The tensor $\hat{\mathbf{G}}_s$ is associated with the deformation induced by growth and can therefore be called the growth tensor. The tensor $\hat{\mathbf{F}}_s^e$ describing the deformation from $\Omega_s^{t,N}$ to Ω_s^t is not related to growth, and is associated with the deformation induced by elasticity. The stress tensor $\hat{\sigma}_s$ is dependent only on the component $\hat{\mathbf{F}}_s^e$ of the deformation gradient:

$$\hat{\sigma}_s = \hat{\sigma}_s(\hat{\mathbf{F}}_s^e) \quad \text{in} \quad \Omega_s^0.$$

Next, we will derive the expression of the growth tensor $\hat{\mathbf{G}}_s$. Let $\hat{\rho}_s^0$ denote the density at time $t = 0$, which is preserved during the deformation from Ω_s^0 to $\Omega_s^{t,N}$, and let $\rho_s = \rho_s(t, x)$ denote the density in Ω_s^t. For a subdomain $V_s^0 \subset \Omega_s^0$ which is deformed to $V_s^{t,N} \subset \Omega_s^{t,N}$ and to $V_s^t \subset \Omega_s^t$, the mass corresponding to $V_s^{t,N}$ and V_s^t are equal, and thus we have

$$\int_{V_s^t} \rho_s(x, t) dx = \int_{V_s^{t,N}} \hat{\rho}_s^0 dX_N.$$

Applying the transformation formula for integrals, and taking into account that from V_s^0 to $V_s^{t,N}$ the density $\hat{\rho}_s^0$ is preserved, we obtain

$$\int_{V_s^0} \hat{\rho}_s(X, t) \hat{J}_s(X, t) dX = \int_{V_s^t} \rho_s(x, t) dx$$
$$= \int_{V_s^{t,N}} \hat{\rho}_s^0 dX_N = \int_{V_s^0} \hat{\rho}_s^0 \hat{J}_s^g(X, t) dX. \qquad (17)$$

Here $\hat{J}_s^g$ is the determinant of the growth tensor $\hat{\mathbf{G}}_s$. If we denote by $\hat{J}_s^e$ the determinant of the tensor $\hat{\mathbf{F}}_s^e$, by (16) we have

$$\hat{J}_s = \hat{J}_s^e \hat{J}_s^g \quad \text{in} \quad \Omega_s^0. \qquad (18)$$

Then from (17), we have

$$\hat{\rho}_s^0 = \hat{\rho}_s \hat{J}_s^e \quad \text{in} \quad \Omega_s^0.$$

Differentiating the above formula with respect to time we have

$$\frac{\partial}{\partial t} (\hat{\rho}_s \hat{J}_s^e) = 0 \quad \text{in} \quad \Omega_s^0. \qquad (19)$$

Recalling (18) and combining (19) with the conservation equation of mass in (4), we have

$$\hat{J}_s \hat{f}_s^g = \frac{\partial}{\partial t}(\hat{\rho}_s \hat{J}_s) = \hat{\rho}_s \hat{J}_s^e \frac{\partial \hat{J}_s^g}{\partial t} \quad \text{in} \quad \Omega_s^0, \tag{20}$$

and (20) can be simplified as

$$\frac{\partial \hat{J}_s^g}{\partial t} = \frac{\hat{f}_s^g}{\hat{\rho}_s} \hat{J}_s^g \quad \text{in} \quad \Omega_s^0. \tag{21}$$

We assume that the growth of plaques in the vessel wall is isotropic, which means that the plaque is growing equally in all directions. Then the growth tensor is written as

$$\hat{\mathbf{G}}_s = \hat{g}_s I \quad \text{in} \quad \Omega_s^0. \tag{22}$$

The scalar function $\hat{g}_s = \hat{g}_s(X, t)$ is called the metric of growth, and we have

$$\hat{J}_s^g = det\hat{\mathbf{G}}_s = \hat{g}^2,$$

where 2 represents the dimension of the space $\mathbb{R}^2$. The formula $dX_N = \hat{J}_s^g dX$ describes how the metric of the reference configuration is changed during the growth process. Now (21) is rewritten as

$$2\frac{\partial \hat{g}_s}{\partial t} = \frac{\hat{f}_s^g}{\hat{\rho}_s} \hat{g}_s \quad \text{in} \quad \Omega_s^0. \tag{23}$$

Remark that the coefficient 2 in front of $\frac{\partial \hat{g}_s}{\partial t}$ represents the dimension of the space. In the three-dimensional setting, it has to be set to 3. In the Lagrangian framework the metric of growth is given by Eq. (23), whereas in the Eulerian framework it is transformed to

$$2\frac{\partial g_s}{\partial t} + 2\mathbf{v}_s \cdot \nabla g_s = \frac{f_s^g}{\rho_s} g_s \quad \text{in} \quad \Omega_s^t. \tag{24}$$

Using the metric of growth and (22), we are able to calculate the tensor $\hat{\mathbf{F}}_s^e$ used in the constitutive equations of $\hat{\sigma}_s$ as follows:

$$\hat{\mathbf{F}}_s^e = \hat{\mathbf{F}}_s \hat{\mathbf{G}}_s^{-1} = \frac{1}{\hat{g}_s} \hat{\mathbf{F}}_s \quad \text{in} \quad \Omega_s^0. \tag{25}$$

To provide the constitutive equations of $\hat{\sigma}_s$, we assume that both the healthy vessel wall and the plaque are hyperelastic, isotropic and incompressible Tang et al. (2004, 2008). In our model, we consider the incompressible neo-Hookean material. The corresponding constitutive equations are then

$$\hat{\sigma}_s = -\hat{p}_s I + \hat{\mu}_s (\hat{\mathbf{F}}_s^e \hat{\mathbf{F}}_s^{eT} - I) \quad \text{in} \quad \Omega_s^0, \tag{26}$$

where $\hat{\mathbf{F}}_s^e$ denotes the deformation of the vessel wall induced by elasticity and is given by (25). For a homogeneous material the shear modulus $\hat{\mu}_s$ is constant. However, the accumulation of foam cells leads to formation of plaques, which have different mechanical properties from the healthy vessel wall Holzapfel et al. (2002), Tang et al. (2004, 2009). Thus the $\hat{\mu}_s$ varies depending on the concentration of foam cells. Analogously to the diffusion coefficient $\hat{D}_s$ defined in (10), Sect. 2.2, we define $\hat{\mu}_s$ by

$$\hat{\mu}_s = \mu_{s,d} + (\mu_{s,h} - \mu_{s,d})e^{-a_2\hat{c}_s^*} \quad \text{in} \quad \Omega_s^0. \tag{27}$$

Here $a_2 > 0$ is a constant, $\mu_{s,d}$ denotes the shear modulus in the diseased vessel wall whereas $\mu_{s,h}$ denotes the shear modulus in the healthy vessel wall.

Finally, we would like to mention that since we model the vessel wall by the incompressible neo-Hookean material, the incompressibility yields

$$\hat{J}_s^e = 1 \quad \text{in} \quad \Omega_s^0.$$

and the system (4) can be further simplified. Since $\hat{J}_s = \hat{J}_s^e \hat{J}_s^g$, and $\hat{J}_s^g = \hat{g}_s^2$, the conservation equation of mass in (4) can be written as

$$\hat{g}_s^2 \hat{f}_s^g = \hat{J}_s^g \hat{f}_s^g = \hat{J}_s \hat{f}_s^g = \frac{\partial}{\partial t}(\hat{J}_s \hat{\rho}_s) = \frac{\partial}{\partial t}(\hat{J}_s^g \hat{\rho}_s) = \frac{\partial}{\partial t}(\hat{g}_s^2 \hat{\rho}_s) \quad \text{in} \quad \Omega_s^0.$$

Combining the upper formula with the equation for the metric of growth (23), we have

$$\frac{\partial \hat{\rho}_s}{\partial t} = 0 \quad \text{in} \quad \Omega_s^0.$$

So in this case, the density of the vessel wall $\hat{\rho}_s$ is independent on time and can be considered as a constant coefficient. Thus, (4) can be simplified as

$$\begin{aligned} \hat{J}_s \hat{\rho}_s \frac{\partial \hat{\mathbf{v}}_s}{\partial t} &= \widehat{\text{div}}(\hat{J}_s \hat{\boldsymbol{\sigma}}_s \hat{\mathbf{F}}_s^{-T}) \quad \text{in} \quad \Omega_s^0 \\ \frac{\partial \hat{\mathbf{u}}_s}{\partial t} &= \hat{\mathbf{v}}_s \quad \text{in} \quad \Omega_s^0. \end{aligned} \tag{28}$$

Combined with the constitutive equations (26), the equations for structural mechanics of the vessel wall (28) are finally obtained. We mention that via (23) and (27) these equations are also coupled with the concentrations $\hat{c}_s$ and $\hat{c}_s^*$.

2.4 Final model

In this section we collect all equations and state the final mathematical model. It has two main parts which are strongly coupled. The fluid-structure interaction problem combines the Navier-Stokes equations (1) with the elastic structure equations (28):

$$\rho_f \frac{\partial \mathbf{v}_f}{\partial t} + \rho_f \mathbf{v}_f \cdot \nabla \mathbf{v}_f = \operatorname{div} \boldsymbol{\sigma}_f \quad \text{in} \quad \Omega_f^t$$

$$\operatorname{div} \mathbf{v}_f = 0 \quad \text{in} \quad \Omega_f^t$$

$$\hat{J}_s \hat{\rho}_s \frac{\partial \hat{\mathbf{v}}_s}{\partial t} = \widehat{\operatorname{div}}(\hat{J}_s \hat{\boldsymbol{\sigma}}_s \hat{\mathbf{F}}_s^{-T}) \quad \text{in} \quad \Omega_s^0$$

$$\frac{\partial \hat{\mathbf{u}}_s}{\partial t} = \hat{\mathbf{v}}_s \quad \text{in} \quad \Omega_s^0,$$

(29)

and is used to describe the fluid dynamics of the blood flow and the structural mechanics of the vessel wall. The transport equations for the biochemical species consist of the equations (6), (7) and (8):

$$\frac{\partial c_f}{\partial t} + \mathbf{v}_f \cdot \nabla c_f - D_f \triangle c_f = 0 \quad \text{in} \quad \Omega_f^t$$

$$\frac{\partial}{\partial t}(\hat{J}_s \hat{c}_s) - \widehat{\operatorname{div}}(\hat{J}_s \hat{\mathbf{F}}_s^{-1} \cdot \hat{D}_s \hat{\mathbf{F}}_s^{-T} \hat{\nabla} \hat{c}_s) = -\hat{J}_s \hat{f}_s^r \quad \text{in} \quad \Omega_s^0$$

$$\frac{\partial}{\partial t}(\hat{J}_s \hat{c}_s^*) = \hat{J}_s \hat{f}_s^r \quad \text{in} \quad \Omega_s^0.$$

(30)

They are used to describe the motion of monocytes, macrophages and foam cells. The process how the accumulation of foam cells leads to plaque growth is described by the equation for the metric of growth:

$$2\frac{\partial \hat{g}_s}{\partial t} = \frac{\hat{f}_s^g}{\hat{\rho}_s} \hat{g}_s \quad \text{in} \quad \Omega_s^0.$$

(31)

The metric of growth determines the constitutive equations for $\hat{\boldsymbol{\sigma}}_s$. The growth function $\hat{f}_s^g$, the reaction function $\hat{f}_s^r$, and the stress tensors $\boldsymbol{\sigma}_f$ and $\hat{\boldsymbol{\sigma}}_s$ are given as

$$\hat{f}_s^g = \gamma \hat{f}_s^r, \quad \hat{f}_s^r = \beta \hat{c}_s \quad \text{in} \quad \Omega_s^0$$

$$\boldsymbol{\sigma}_f = -p_f I + \rho_f \nu (\nabla \mathbf{v}_f + \nabla \mathbf{v}_f^T) \quad \text{in} \quad \Omega_f^t$$

$$\hat{\boldsymbol{\sigma}}_s = -\hat{p}_s I + \hat{\mu}_s (\hat{\mathbf{F}}_s^e \hat{\mathbf{F}}_s^{eT} - I) \quad \text{in} \quad \Omega_s^0$$

$$\hat{\mathbf{F}}_s^e = \hat{\mathbf{F}}_s \hat{\mathbf{G}}_s^{-1} = \frac{1}{\hat{g}_s} \hat{\mathbf{F}}_s \quad \text{in} \quad \Omega_s^0.$$

(32)

The diffusion coefficients $\hat{D}_s$ and the shear modulus $\hat{\mu}_s$ are given by

$$\hat{D}_s = D_{s,d} + (D_{s,h} - D_{s,d})e^{-a_1 \hat{c}_s^*} \quad \text{in} \quad \Omega_s^0$$

$$\hat{\mu}_s = \mu_{s,d} + (\mu_{s,h} - \mu_{s,d})e^{-a_2 \hat{c}_s^*} \quad \text{in} \quad \Omega_s^0.$$

(33)

The model is closed by the initial and boundary conditions from Eqs. (29) and (30)

$$\mathbf{v}_f|_{t=0} = \mathbf{v}_f^0, \quad c_f|_{t=0} = c_f^0 \quad \text{in} \quad \Omega_f^0$$
$$\mathbf{v}_f = \mathbf{v}_f^D, \quad c_f = c_f^D \quad \text{on} \quad \Gamma_{f,in}$$
$$\mathbf{v}_f = 0, \quad \nabla c_f \cdot \mathbf{n}_f = 0 \quad \text{on} \quad \Gamma_{f,wall}$$
$$\rho_f \nu \nabla \mathbf{v}_f \cdot \mathbf{n}_f - p_f \mathbf{n}_f = 0, \quad \nabla c_f \cdot \mathbf{n}_f = 0 \quad \text{on} \quad \Gamma_{f,out}$$
$$\hat{g}_s|_{t=0} = 1 \quad \text{in} \quad \Omega_s^0 \tag{34}$$
$$\hat{\mathbf{v}}_s|_{t=0} = 0, \quad \hat{\mathbf{u}}_s|_{t=0} = 0 \quad \text{in} \quad \Omega_s^0$$
$$\hat{c}_s|_{t=0} = 0, \quad \hat{c}_s^*|_{t=0} = 0 \quad \text{in} \quad \Omega_s^0$$
$$\hat{\mathbf{v}}_s = 0, \quad \hat{\mathbf{u}}_s = 0 \quad \text{on} \quad \Gamma_{s,in} \cup \Gamma_{s,wall} \cup \Gamma_{s,out}$$
$$\hat{\mathbf{F}}_s^{-T} \hat{\nabla} \hat{c}_s \hat{\mathbf{F}}_s^{-T} \cdot \mathbf{N}_s = 0 \quad \text{on} \quad \Gamma_{s,in} \cup \Gamma_{s,wall} \cup \Gamma_{s,out},$$

as well as the transmission conditions on the interface Γ^t

$$\mathbf{v}_f = \mathbf{v}_s, \quad \boldsymbol{\sigma}_f \cdot \mathbf{n}_f + \boldsymbol{\sigma}_s \cdot \mathbf{n}_s = 0$$
$$D_f \nabla c_f \cdot \mathbf{n}_f + D_s \nabla c_s \cdot \mathbf{n}_s = 0 \tag{35}$$
$$D_f \nabla c_f \cdot \mathbf{n}_f + \zeta (c_f - c_s) = 0.$$

Here $\mathbf{N}_s$ is the unit outer normal vector of $\Gamma_{s,in} \cup \Gamma_{s,wall} \cup \Gamma_{s,out}$ with respect to Ω_s^0, and the last boundary condition in (34) is obtained from the boundary condition $\nabla c_s \cdot \mathbf{n}_s = 0$ by using the transformation formula. Based on these equations, in the next section numerical simulations are performed to investigate the formation and evolution of plaques.

3 Numerical simulation

3.1 Numerical methods

For the numerical computation of the solution we choose a monolithic framework, where the coupled equations in the fluid and solid domains are solved simultaneously. However, the equations in different domains are given in different frameworks, making a common solution approach challenging. The equations in the fluid domain are formulated in the Eulerian framework, where Ω_f^t is changing in time due to the movement of the interface Γ^t. The equations in the solid domain are given in the Lagrangian framework, where the domain Ω_s^0 is fixed. For numerical simulations this means that different meshes are needed in different subdomains as well as in different time steps. To avoid this difficulty, we employ the Arbitrary Lagrangian-Eulerian (ALE) framework, in which the fluid domain is transformed to a fixed one by the ALE mapping, and all the equations in the fluid domain are rewritten in the fixed domain Ω_f^0. To construct the ALE mapping, we define the artificial variable $\hat{\mathbf{u}}_f$, which is the harmonic extension of the displacement $\hat{\mathbf{u}}_s$ to Ω_f^0. In this way, both of the subdomains Ω_f^0 and Ω_s^0 are fixed, and a common mesh can be used for the spatial discretization in each time step. For a general introduction to the ALE method for fluid-structure interaction problems, see e.g. Dunne et al. (2010).

Based on the variational formulation in the ALE framework, numerical simulations of our model are performed by using the finite element library Gascoigne, see Richter (2011). Temporal discretization is achieved with finite difference schemes, more precisely, we choose the implicit backward Euler scheme, which is sufficiently stable and accurate. Spatial discretization is based on the Galerkin finite element method, and some stabilization techniques similar to those in Johnson (1987), Richter (2011) are used to treat Stokes equations and convection-dominated problems. The discretized problem is highly nonlinear, and it is linearized and solved by the Newton method.

Finally, we would like to emphasize that the formation and evolution of plaques are long time processes, and we have to choose a large time step for the temporal discretization. At this time scale the time differences of the quantities in the fluid domain, such as the velocity $\mathbf{v}_f$ and the concentration c_f, can be neglected. Therefore, we remove the terms containing the time derivatives of $\mathbf{v}_f$ and c_f in Eqs. (29) and (30), and consider for the numerical calculations the reduced system:

$$
\begin{aligned}
\rho_f \mathbf{v}_f \cdot \nabla \mathbf{v}_f &= \operatorname{div} \boldsymbol{\sigma}_f \quad \text{in} \quad \Omega_f^t \\
\operatorname{div} \mathbf{v}_f &= 0 \quad \text{in} \quad \Omega_f^t \\
\hat{J}_s \hat{\rho}_s \frac{\partial \hat{\mathbf{v}}_s}{\partial t} &= \widehat{\operatorname{div}}(\hat{J}_s \hat{\boldsymbol{\sigma}}_s \hat{\mathbf{F}}_s^{-T}) \quad \text{in} \quad \Omega_s^0 \\
\frac{\partial \hat{\mathbf{u}}_s}{\partial t} &= \hat{\mathbf{v}}_s \quad \text{in} \quad \Omega_s^0 \\
\mathbf{v}_f \cdot \nabla c_f - D_f \triangle c_f &= 0 \quad \text{in} \quad \Omega_f^t \\
\frac{\partial}{\partial t}(\hat{J}_s \hat{c}_s) - \widehat{\operatorname{div}}(\hat{J}_s \hat{\mathbf{F}}_s^{-1} \cdot D_s \hat{\mathbf{F}}_s^{-T} \hat{\nabla} \hat{c}_s) &= -\hat{J}_s \hat{f}_s^r \quad \text{in} \quad \Omega_s^0 \\
\frac{\partial}{\partial t}(\hat{J}_s \hat{c}_s^*) &= \hat{J}_s \hat{f}_s^r \quad \text{in} \quad \Omega_s^0 \\
2 \frac{\partial \hat{g}_s}{\partial t} &= \frac{\hat{f}_s^g}{\hat{\rho}_s} \hat{g}_s \quad \text{in} \quad \Omega_s^0 .
\end{aligned}
\tag{36}
$$

3.2 Parameters

In numerical simulations, we consider a computational domain in two-dimensional space, see Fig. 4, the characteristics of which are given in Table 1. It consists of two parts, the fluid domain Ω_f^0 and the solid domain Ω_s^0. On the interface $\Gamma_1^0 \cup \Gamma_2^0$, the dashed part denotes the interface Γ_1^0 which is permeable for the monocytes. Additionally, there is another dashed line in Ω_s^0, and we consider the layer between the interface and this dashed line as endothelial cells and smooth muscle cells which are not affected a lot by plaque formation. In this transition layer, chemical reactions rarely take place, so the monocytes will not be converted to foam cells. This fact is confirmed by our medical partners.

The parameters of the model and the initial conditions are listed in Table 2. They are taken from the medical literature e.g. Barrett et al. (2010), Fung (1984), Li et al.
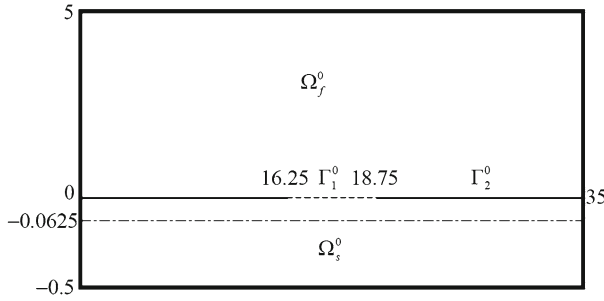
Fig. 4 Configuration of the computational domain in the ALE framework

Table 1 Characteristics of the computational domain

Fluid domain Ω_f^0	Length 35.0 mm
	Width 5.0 mm
Solid domain Ω_s^0	Length 35.0 mm
	Width 0.5 mm
Part of interface permeable for monocytes Γ_1^0	Length 2.5 mm
Transition layer	Width 0.0625 mm

Table 2 Parameter values and initial conditions

Density ρ_f	0.0010 g/mm^3
Kinematic viscosity ν	3.0 mm^2/s
Diffusion coefficient D_f	1.0×10^{-6} mm^2/s
Density ρ_s	0.00106 g/mm^3
Growth coefficient γ	1.0×10^{-6} g
Shear modulus μ_s	$\mu_{s,h} = 1.0 \times 10^5$ g/mm s^2
	$\mu_{s,d} = 0.05 \times \mu_{s,h}$
Diffusion coefficient D_s	$D_{s,h} = 1.0 \times 10^{-7}$ mm^2/s
	$D_{s,d} = 5.0 \times D_{s,h}$
Reaction coefficient β	1.0×10^{-7}/s
Permeability of the interface	$\zeta = 1.0 \times 10^{-4}$ mm/s on Γ_1^0
	$\zeta = 0$ on Γ_2^0
Initial velocity v_f^0	$48x(5-x)$ mm/s
Initial concentration c_f^0	540.0/mm^3

(2006), Quarteroni et al. (2001), Robertson et al. (2008), Tang et al. (2004), Zamir (2005).

The shear modulus μ_s is defined by (27), and the diffusion coefficient D_s is defined in (10). We remark that the elastic coefficient decreases and the diffusion coefficient increases in the diseased vessel wall, because as the plaque is formed, the diseased tissue becomes softer and easier for molecules to diffuse. Concerning the reaction coefficient, we set a constant value β under the lower dashed line and choose a much

smaller amount between the interface and the lower dashed line, so the reaction can be neglected in this transition layer of Ω_s^0. Finally on the interface, we set a constant value ζ on Γ_1^0 and 0 on Γ_2^0. The corresponding initial and boundary conditions are given as (34). Especially the initial velocity profile of the blood flow is a parabola Fung (1984), and the initial value of the concentration of monocytes in Ω_f^0 is a positive constant.

3.3 Numerical results

After performing numerical computations in the ALE framework, we use the software Paraview to visualize the numerical results in the whole domain $\Omega_f^t \cup \Omega_s^t$, with respect to the Eulerian framework, so that we can observe not only the evolution of the solution components (displacement, velocity, concentrations), but also the motion of the domain when the plaque is formed. The maximal simulation time is $t = 4.5 \times 10^7 s$ (521 days). The motion of the interface and the x-component of the velocity are visualized at the time points $t = 0s$, $t = 3.0 \times 10^7 s$ (347 days), and $t = 4.5 \times 10^7 s$ (521 days). All other computed quantities are visualized at the time points $t = 0s$, $t = 3.0 \times 10^7 s$ (347 days), $t = 3.75 \times 10^7 s$ (434 days), and $t = 4.5 \times 10^7 s$ (521 days). The results are obtained on a locally refined mesh, having 2 levels of local refinement near the interface.

#### 3.3.1 Evolution of velocity and displacement

Figure 5 shows the motion of the interface Γ^t (indicated by the white line) and the evolution of the x-component of the velocity in the domain $\Omega_f^t \cup \Omega_s^t$. At initial time, the interface is parallel to the upper and lower boundary of the domain Ω. When time passes, the interface moves due to the formation and growth of the plaque in Ω_s^t. This motion is presented in Fig. 6, where the y-component of the displacement in the solid domain Ω_s^t is visualized. We can see that after 4.5×10^7 seconds Ω_s^t has been deformed to form a hump around the permeable interface Γ_1^t. The computations for the x-component of the displacement led to negligibly small values.

3.3.2 Evolution of concentrations

Figures 7 and 8 show how plaque formation and growth are induced by the penetration of monocytes and the accumulation of foam cells. Figure 7 presents the evolution of concentration of monocytes c_f in the fluid domain Ω_f^t. When the plaque formation starts, the concentration of monocytes decreases mainly downstream of the permeable part of the interface, denoted by Γ_1^t. This demonstrates that the decrease in c_f is due to penetration of monocytes into the vessel wall. At the same time foam cells are formed with a concentration c_s^*, see Fig. 8. We remark that the region with high c_s^* is separated from the fluid domain Ω_f^t by a thin layer, where the concentration of foam cells is low. This is in agreement with observations communicated to us by our medical partner M. Henerici (Neurologische Universitätsklinik Mannheim).

$t = 0,\ max\ v_x = 300 mm/s$
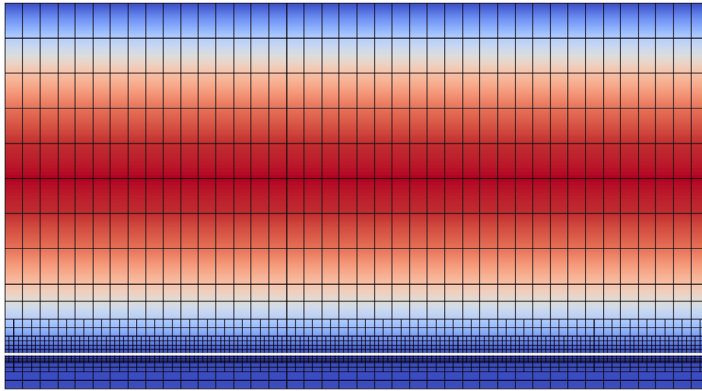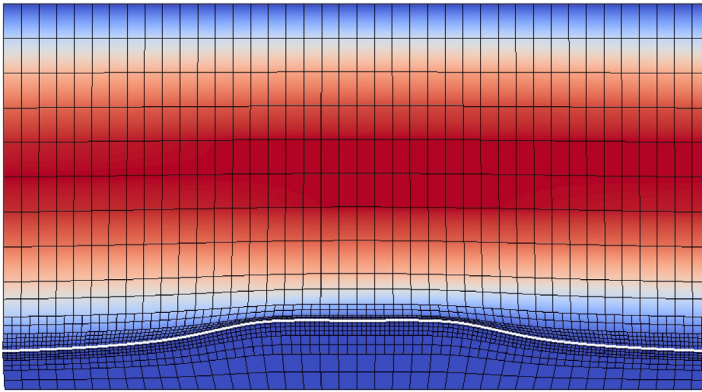
$t = 3.0 \times 10^7 s,\ max\ v_x = 315 mm/s$
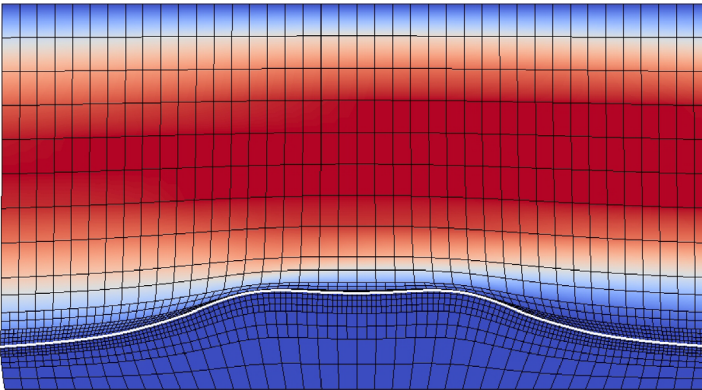
$t = 4.5 \times 10^7 s,\ max\ v_x = 334.5 mm/s$

Fig. 5 Motion of the interface and evolution of the x-component of the velocity in the domain $\Omega_f^t \cup \Omega_s^t$. Mesh refinement level $= 2$. The *white line* indicates the interface. *Red color* denotes high value, while *blue color* denotes low value. The domain size at the initial time is [12.5 mm, 22.5 mm] $\times$ [-0.5 mm, 5 mm]

$t = 0, \ max \ u_{s,y} = 0mm$

$t = 3.0 \times 10^7 s, \ max \ u_{s,y} = 0.493mm$

$t = 3.75 \times 10^7 s, \ max \ u_{s,y} = 0.685mm$

$t = 4.5 \times 10^7 s, \ max \ u_{s,y} = 0.915mm$
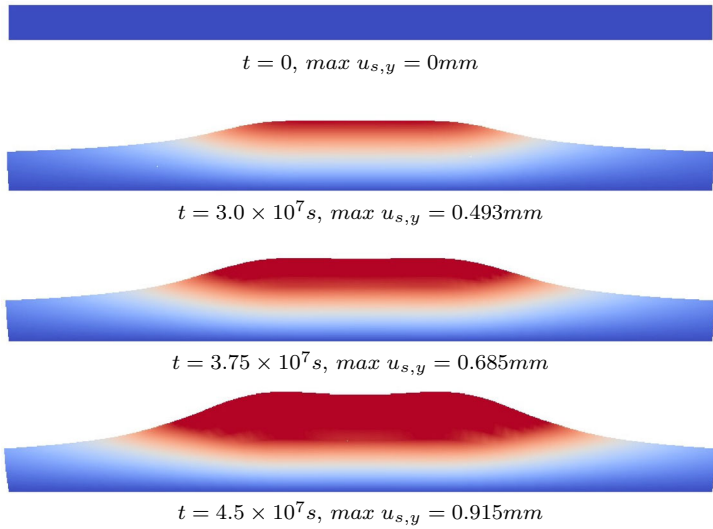
Fig. 6 Evolution of the y-component of the displacement in the solid domain Ω_s^t. Mesh refinement level $= 2$. *Red color* denotes high value, while *blue color* denotes low value. The domain size at the initial time is [12.5 mm, 22.5 mm] $\times$ [-0.5 mm, 0 mm]

$t = 0$

$t = 3.0 \times 10^7 s$

$t = 3.75 \times 10^7 s$

$t = 4.5 \times 10^7 s$
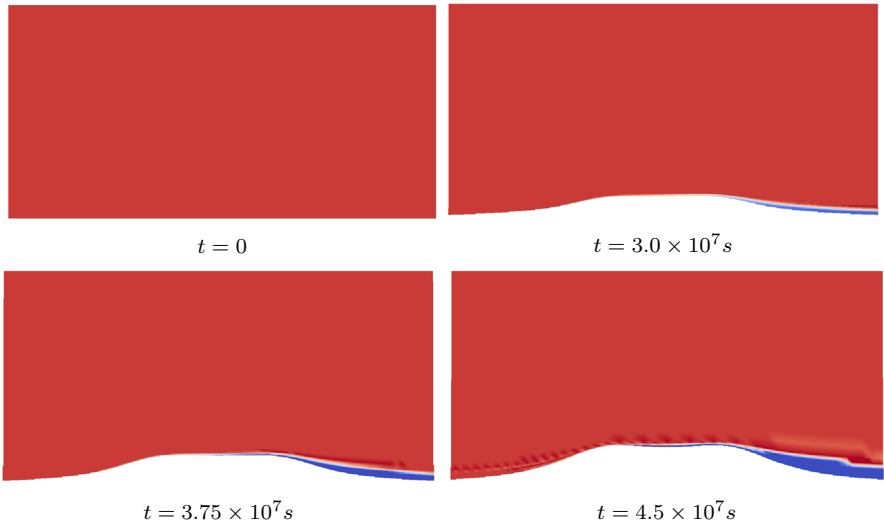
Fig. 7 Evolution of concentration of monocytes in the fluid domain Ω_f^t. Mesh refinement level $= 2$. *Red color* denotes high value, while *blue color* denotes low value. The domain size at the initial time is [12.5 mm, 22.5 mm] $\times$ [0 mm, 5 mm]
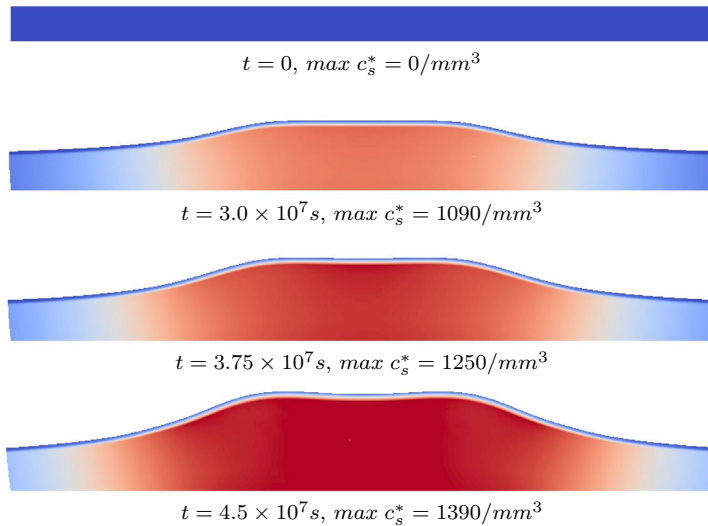
Fig. 8 Evolution of concentration of foam cells in the solid domain Ω_s^t. Mesh refinement level = 2. *Red color* denotes high value, while *blue color* denotes low value. The domain size at the initial time is [12.5 mm, 22.5 mm] × [−0.5 mm, 0 mm]

3.3.3 Evolution of principal stress

Figure 9 shows that, when the plaque is growing, the principal stress $\sigma_{s,p}$, (given by the largest eigenvalue of the stress tensor σ_s) reaches its maximum value around the hump of the interface.

3.3.4 Discussion

We remark that the simulation shows slow evolution of a plaque in the region where the vessel wall allows the penetration of monocytes, the duration is of order of 521 days. This indicates that time and space scales are at an adequate level. However, we have to emphasize that here the blood inflow is assumed to be constant in time. In an improved model, a correction due to time oscillatory inflow will be necessary.

It is at first surprising, that for realistic parameters spatial oscillations (two humps) appear in the form of the plaque, where one expects at first simple bell shapes. In fact, bell shapes can be observed in other, less realistic parameter regimes. These oscillations are no numerical artifacts, indeed such oscillations can be observed in real plaques.

Our model is based on the assumption that accumulation of foam cells leads to volume growth. Figure 9 shows that the concentration of foam cells is very high at the place of large deformation, which is consistent with our modeling assumption. The fact that the principal stress $\sigma_{s,p}$ reaches its maximal values around the hump of the interface, indicates that these regions are very prone to plaque rupture. In contrast, $\sigma_{s,p}$ is smaller inside the plaque, even though this part is also under a large deformation.
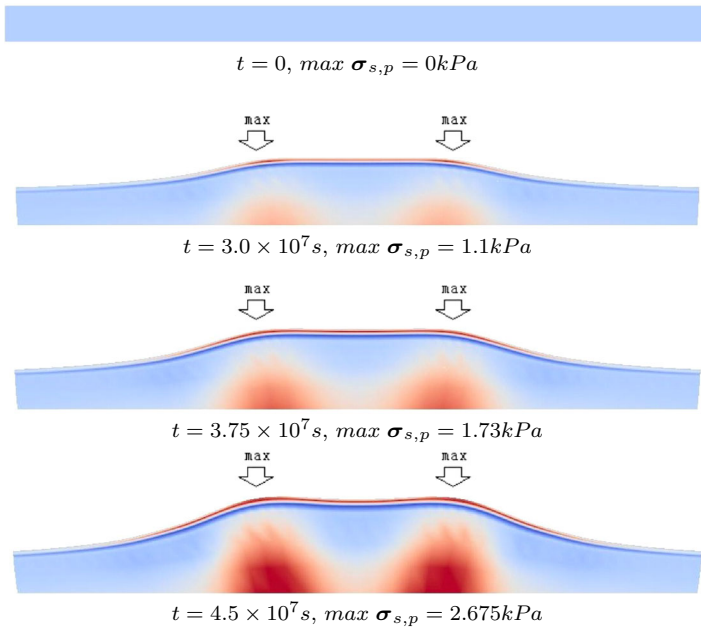
Fig. 9 Evolution of principal stress in the solid domain Ω_s^t. Mesh refinement level = 2. *Red color* denotes high value, while *blue color* denotes low value. The maximum value is reached around the hump of the interface. The domain size at the initial time is [12.5 mm, 22.5 mm] × [−0.5 mm, 0 mm]

Remark 1 The shear stress plays an important role for the dynamics of biological cells. Similar to chemical or electrical signaling, shear stress may initiate and regulate cellular processes. E.g. it may influence the permeability of the endothelial layer in blood vessels. The wall shear stress in the region of the plague can be large. Therefore we have to expect there an increased permeability of the vessel wall for the monocytes, as we have assumed, without modelling this process explicitly. Taking into account that the vessel wall in the region of the plaque develops humps, it can be expected that wall shear stress is going to oscillate in direction of the flow, as it is seen in Fig. 10.

4 Concluding remarks

This paper can be considered as a feasibility study, demonstrating that it is possible, to model and calculate the evolution of plaques in arteries. As a first step, a reduced system is studied. It is an example for systems, modeling interaction of fluid flow transporting material in a vessel with the flexible vessel wall, incorporating material and changing its shape and mechanical behavior. The focus in this paper is on the modeling part and on the presentation and discussion of the simulation results.

The results for the reduced model derived in this paper encourage to improve the modelling and simulation by including

– Available further information on the dynamics of involved cell populations,
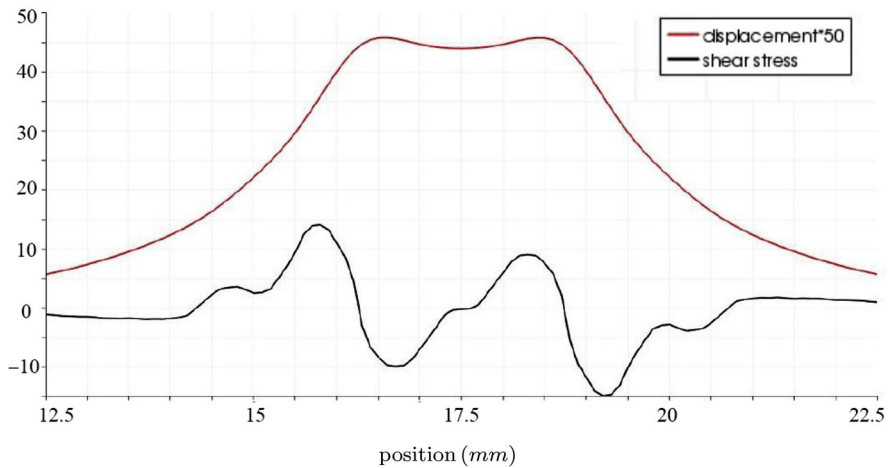– The formation of lipid cores and fibrous caps,

Fig. 10 Distribution of wall shear stress in Pa (*black line*) and displacement$\times 50$ in mm (*red line*) on the interface between blood flow and vessel wall in the plaque region

– The rupture of the plaque. See also Hahn and Schwartz (2009), Kalita and Schaefer (2008), Quarteroni et al. (2000).

A challenge as well to mathematical analysis as to numerics poses the following fact. Two processes of rather different time scale are interacting: the oscillation of the blood flow on the scale of seconds, caused by the heart, pumping blood through its vessel system, and the growth of plaques which is rather on the scale of months. An approximation of the model has to be found to compute the evolution of plaque. A complete mathematical analysis of the developed model system is necessary for further progress. It remains a major problem to estimate the necessary parameters from real data. Close cooperation with experts in biomechanics, biophysics and biochemistry in medicine is required, in particular to set up experiments providing appropriate data. Developing a method to identify the moment, in which a rupture of a plaque might happen, is still remaining an aim and not yet a result.

Processes considered in this paper are also arising as components in other medically relevant processes, e.g. in inflammation as a protective response of the immune system to harmful stimuli. A large research area opens up for mathematical modelling and simulation. Finally, we mention that the mathematics developed for plaque formation is portable to other areas of research and applications, e.g. to material sciences.

References

Ambrosi D, Mollica F (2002) On the mechanics of a growing tumor. Int J Eng Sci 40(12):1297–1316
Barrett KE, Boitano S, Barman SM, Brooks HL (2010) Ganongs review of medical physiology, 23rd edn. McGraw Hill Professional, USA

Boyd J, Buick JM, Green S (2007) Analysis of the Casson and Carreau-Yasuda non-Newtonian blood models in steady and oscillatory flows using the lattice Boltzmann method. Phy Fluids 19(9):093103

Ciarlet PG (1988) Mathematical Elasticity, vol.I: Three-Dimensional Elasticity. North-Holland, Amsterdam

Doktorski I (2007) Mechanical model for biofilm growth phase. PhD thesis, University of Heidelberg

Dunne T, Rannacher R, Richter T (2010) Numerical simulation of fluid-structure interaction based on monolithic variational formulations. Fundamental Trends in Fluid-Structure Interaction., vol 1 of Contemporary Challenges in Mathematical Fluid Dynamics and Its ApplicationsWorld Scientific, Singapore, pp 1-75

El Khatib N, Génieys S, Volpert V (2007) Atherosclerosis Initiation Modeled as an Inflammatory Process. Math Model Nat Phenom 2:126–141

Fasano A, Santos RF, Sequeira A (2011) Blood coagulation: a puzzle for biologists, a maze for mathematicians. In: Ambrosi D, Quarteroni A, Rozza G (eds) Modelling of physiological flows. Springer-Verlag, Italia, pp 41–75

Fernández MA, Formaggia L, Gerbeau J-F, Quarteroni A (2009) The derivation of the equations for fluids and structure. Cardiovascular Mathematics., vol 1, Springer, Milan, pp 77-121

Fogelson AL (1992) Continuum models of platelet aggregation: formulation and mechanical properties. SIAM J Appl Math 52(4):1089–1110

Formaggia L, Moura A, Nobile F (2007) On the stability of the coupling of 3D and 1D fluid-structure interaction models for blood flow simulations. ESAIM. Math Model Num Anal 41(04):743–769

Fung YC (1984) Biodynam Circ. Springer-Verlag, New York

Hahn C, Schwartz MA (2009) Mechanotransduction in vascular physiology and atherogenesis. Nat Rev Mol Cell Biol 10:53–62

Holzapfel G (2000) Nonlinear solid mechanics, a continuum approach for engineering. John Wiley and Sons, Chichester

Holzapfel GA, Stadler M, Schulze-Bauer CAJ (2002) A layer-specific three-dimensional model for the simulation of balloon angioplasty using magnetic resonance imaging and mechanical testing. Ann Biomed Eng 30:753–767

Hron J, Madlik M (2007) Fluid-structure interaction with applications in biomechanics. Nonlinear Anal Real World Appl 8:1431–1458

Humphrey JD (2002) Cardiovascular solid mechanics, cells, tissues, and organs. Springer, NewYork

Ibragimov AI, McNeal CJ, Ritter LR, Walton JR (2005) A mathematical model of atherogenesis as an inflammatory response. Math Med Biol 22(4):305–333

Janela J, Moura A, Sequeira A (2010) A 3D non-Newtonian fluid-structure interaction model for blood flow in arteries. J Comp Appl Math 234(9):2783–2791

Johnson C (1987) Numerical solution of partial differential equations by the finite element method. Cambridge University Press, Cambridge

Jones GW, Chapman SJ (2012) Modeling growth in biological materials. SIAM Rev 54(1):52–118

Kalita P, Schaefer R (2008) Mechanical models of artery walls. Arch Comp Methods Eng 15:1–36

Li ZY, Howarth SPS, Tang T, Gillard JH (2006) How critical is fibrous cap thickness to carotid plaque stability? Stroke 37(5):1195–1199

Ougrinovskaia A, Thompson R, Myerscough M (2010) An ODE model of early stages of atherosclerosis: mechanisms of theinflammatory response. Bull Math Biol 72:1534–1561

Pasterkamp G, Falk E (2000) Atherosclerotic plaque rupture: an overview. J Clin Basic Cardiol 3:81–86

Quarteroni A, Formaggia L (2004) Mathematical modelling and numerical simulation of the cardiovascular system. In: Handbook of numerical analysis 12. Elsevier, Amsterda, pp 3-127

Quarteroni A, Tuveri M, Veneziani A (2000) Computational vascular fluid dynamics: problems, models and methods. Comp Visual Sci 2:163–197

Quarteroni A, Veneziani A, Zunino P (2001) Mathematical and numerical modeling of solute dynamics in blood flow and arterial walls. SIAM J Numer Anal 39(5):1488–1511

Rajagopal KR, Srinivasa AR (2004) On thermomechanical restrictions of continua. In: Proceedings of the Royal Society of London A: Mathematical, Physical and Engineering Sciences. 460, The Royal Society, pp 631-651

Richter T (2011) Gascoigne. Lecture Notes, University of Heidelberg, http://numerik.uni-hd.de/richter/SS11/gascoigne/index.html

Robertson AM (2008) Review of relevant continuum mechanics. In: Hemodynamical flows: modeling, analysis and simulation. Springer, pp 1-62

Robertson AM, Sequeira A, Kameneva MV (2008) Hemorheology. In: Hemodynamical flows: modeling, analysis and simulation. Springer, pp 63-120

Tang D, Yang C, Kobayashi S, Zheng J, Woodard PK, Teng Z, Billiar K, Bach R, Ku DN (2009) 3D MRI-based anisotropic FSI models with cyclic bending for human coronary atherosclerotic plaque mechanical analysis. J. Biomech. Eng. 131(6):061010

Tang D, Yang C, Mondal S, Liu F, Canton G, Hatsukami TS, Yuan C (2008) A negative correlation between human carotid atherosclerotic plaque progression and plaque wall stress: In vivo MRI-based 2D/3D FSI models. J Biomech 41(4):727–736

Tang D, Yang C, Zheng J, Woodard PK, Sicard GA, Saffitz JE, Yuan C (2004) 3D MRI-based multicomponent FSI models for atherosclerotic plaques. Ann Biomed Eng 32:947–960

Turek S, Hron J, Madlik M, Razzaq M, Wobker H, Acker JF (2010) Numerical Simulation and Benchmarking of a Monolithic Multigrid Solver for Fluid-Structure Interaction Problems with Application to Hemodynamics. Fluid Structure Interaction II, Springer-Berlin-Heidelberg, pp 193-220

VanEpps JS, Vorp DA (2007) Mechanopathobiology of atherogenesis: a review. J Surg Res 142:202–217

Weller F (2008) Platelet deposition in non-parallel flow. J Math Biol 57:333–359

Weller F, Neuss-Radu M, Jäger W (2013) Analysis of a free boundary problem modeling thrombus growth. SIAM J Math Anal 45:809–833

Wick T (2011) Fluid-structure interactions using different mesh motion techniques. Comp Struct 89:1456–1467

Yang Y, Richter T, Jäger W, Neuss-Radu M. An ALE approach to mechano-chemical processes in fluid-structure interactions (in preparation)

Zamir M (2005) The physics of coronary blood flow, series: biological and medical physics, biomedical engineering. Springer, New York

Zohdi TI, Holzapfel GA, Berger SA (2004) A phenomenological model for atherosclerotic plaque growth and rupture. J Theor Biol 227:437–443